actuators

MDPI

Article

Master Cylinder Pressure Control Based on Piecewise-SMC in Electro-Hydraulic Brake System

Cong Liang [1], Xing Xu [1,*], Hui Deng [1], Chuanlin He [1], Long Chen [1] and Yan Wang [2]

[1] Automotive Engineering Research Institute, Jiangsu University, Zhenjiang 212013, China; cong@ujs.edu.cn (C.L.); deng_hui3@leapmotor.com (H.D.); 2112204003@stmail.ujs.edu.cn (C.H.); chenlong@ujs.edu.cn (L.C.)

[2] Department of Industrial and Systems Engineering, The Hong Kong Polytechnic University, Hong Kong, China; yanjack.wang@polyu.edu.hk

* Correspondence: xuxing@ujs.edu.cn

Abstract

This paper focuses on enhancing master cylinder pressure control in pressure-sensorless Electro-Hydraulic Brake (EHB) systems. A novel control strategy is developed, integrating a Piecewise Sliding Mode Controller (Piecewise-SMC) with an Extended Sliding Mode Observer (ESMO) based on a newly derived pressure–position–velocity model that accounts for rack position and velocity effects. To handle external disturbances and parameter uncertainties, the ESMO provides accurate pressure estimation. The nonlinear EHB model is approximated piecewise linearly to facilitate controller design. The proposed Piecewise-SMC regulates motor torque to achieve precise pressure tracking. Experimental validation under step-change braking conditions demonstrates that the Piecewise-SMC reduces response time by 31.8%, overshoot by 35.8%, and tracking root mean square error by 9.6% compared to traditional SMC, confirming its effectiveness and robustness for pressure-sensorless EHB applications.

Keywords: EHB; pressure estimation; piecewise modeling; sliding mode control; pressure–position–velocity characteristics

Academic Editor: Ioan Ursu

Received: 16 June 2025
Revised: 13 August 2025
Accepted: 22 August 2025
Published: 24 August 2025

Citation: Liang, C.; Xu, X.; Deng, H.; He, C.; Chen, L.; Wang, Y. Master Cylinder Pressure Control Based on Piecewise-SMC in Electro-Hydraulic Brake System. *Actuators* **2025**, *14*, 416. https://doi.org/10.3390/act14090416

1. Introduction

Electric vehicles' shift toward intelligent functionalities has positioned Brake-by-Wire (BBW) as a core technology, with Electro-Hydraulic Brake (EHB) emerging as the dominant solution due to its integration of hydraulic advantages with high responsiveness and reliability [1–4]. However, the EHB's nonlinear electromechanical–hydraulic dynamics, influenced by temperature, fluid properties, and friction, pose significant challenges for precise control under increasingly stringent performance and safety demands [5–7].

To cope with the nonlinearities and uncertainties of EHB systems, diverse pressure-control strategies have been developed [8–10]. Jiang et al. [11] proposed a pressure-based sliding mode control (SMC) with experimentally identified dynamic friction parameters. Xiong et al. [12] developed an adaptive SMC with ideal state feedback and integral anti-windup, enhancing tracking performance but remaining sensitive to pressure fluctuations. A quintessential challenge in conventional SMC is the inherent trade-off between robustness and control chattering, which arises from using a conservative, high-gain switching term to handle system uncertainties. Chen et al. [13] employed a disturbance observer to estimate unmeasurable states and disturbances, proposing an optimized feedforward-enhanced

MPC that outperformed conventional MPC. Although these methods have achieved significant progress in robustness, tracking accuracy, and dynamic response, they still rely on pressure sensors, making them susceptible to measurement noise, drift, and installation constraints [14–16]. Overall, while existing strategies address specific nonlinear effects, their dependence on direct pressure measurement limits adaptability and long-term reliability, indicating the need for sensor-independent or sensor-robust control solutions.

In response to this need, research has increasingly focused on developing reliable master cylinder (MC) pressure estimators, as they form the cornerstone of sensorless control [17,18]. Earlier studies by Shi et al. [19] and Wei et al. [20] developed MC pressure models and signal fusion estimators, improving reliability under dynamic conditions but lacking integration with robust closed-loop control. Evidently, achieving the high accuracy and robustness required for closed-loop control necessitates more advanced observer design concepts. Significant progress in observer design in other fields has provided valuable inspiration. Finite-time adaptive sliding mode observers have shown significant error reductions in hydraulic manipulator control [21]. Likewise, second-order sliding mode observers improve vehicle lateral force estimation by accurately capturing nonlinear tire–road interactions, outperforming traditional filters with up to 99% error reduction and strong robustness [22].

Building on the foundation of reliable pressure estimation, the integrated control strategies that effectively leverage this estimated information [23–25] can be developed. Han's group [26,27] developed estimators and controllers informed by actuator and vehicle dynamics to reduce model sensitivity and improve robustness across operating conditions. Zhao et al. [28] employed a sliding mode observer to replace pressure sensors for coordinated booster–ABS control and proposed an adaptive MC pressure estimation–control framework combining multiple MC pressure estimation techniques. Collectively, these control-oriented approaches demonstrate that estimation–control integration is achievable, but robust adaptation to diverse real-world conditions is still an open challenge.

To provide a clear overview of this progression, Table 1 compares the key strategies discussed, highlighting their respective strengths and unresolved limitations. As the comparative analysis in Table 1 reveals, existing EHB control strategies exhibit limitations in robustness, largely because the fundamental dynamics of MC pressure remain a key but under-addressed research area. To confront this challenge, this paper introduces a Piecewise Sliding Mode Controller (Piecewise-SMC) framework that integrates advancements in modeling, estimation, and control:

(1) A novel position–velocity–pressure (P–V–P) relationship is formulated to provide a more accurate dynamic model of the system.
(2) An Extended Sliding Mode Observer (ESMO) is designed to robustly estimate pressure against nonlinearities, disturbances, and uncertainties.
(3) A Piecewise-SMC is developed, which leverages a piecewise linear model to significantly mitigate chattering and enhance control performance.

Table 1. Comparative analysis with advanced related works.

Approach	Representative Works	Key Strengths	Core Limitations	Contributions of This Study
Advanced Sensor-Based Control	Jiang et al. [11], Xiong et al. [12], Chen et al. [13]	Effectively addresses nonlinearities, such as friction and saturation, enhancing dynamic response and tracking accuracy.	Fundamentally relies on physical pressure sensors, making the system susceptible to noise and drift, which limits long-term reliability and adaptability.	Eliminates the dependency on physical sensors from the ground up through a sensorless estimation-and-control framework.

Table 1. *Cont.*

Approach	Representative Works	Key Strengths	Core Limitations	Contributions of This Study
MC Pressure Estimation Models	Shi et al. [19], Wei et al. [20]	Established initial master cylinder pressure estimation models, verifying the feasibility of a sensorless approach.	1. Limited to the estimation level, lacking integration with a closed-loop control system. 2. Insufficient robustness against system uncertainties and disturbances.	Achieves high-fidelity estimation for closed-loop control by designing a robust ESMO observer grounded in a more accurate P–V–P physical model.
Integrated Estimation and Control Strategies	Han's group [26,27], Zhao et al. [28]	Achieved estimation–control integration, validating the feasibility of an integrated framework and introducing modern control theories.	Robust adaptation under severe parameter uncertainties or actuator degradation remains an open challenge.	Proposes a Piecewise Sliding Mode Controller that embeds a piecewise model into the control law, enhancing robustness and adaptability while significantly mitigating chattering.

2. Analysis and Modeling of the EHB System

The EHB system (Figure 1) integrates the power supply, BCU, BLDC motor, transmission, hydraulic reservoir, master cylinder, and HCU. During braking, pedal input is processed by the ECU to command motor-driven rack–gear actuation of the master cylinder piston, generating hydraulic pressure. The BCU regulates pressure via estimator feedback, while the HCU modulates flow to wheel cylinders for braking force generation.

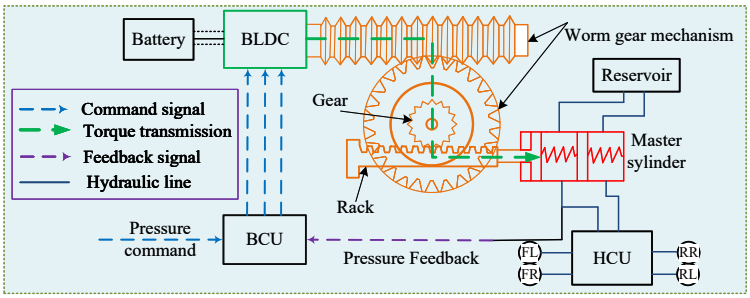

Figure 1. Schematic diagram of the EHB system.

To enable efficient control algorithm design, the actuator dynamics of the EHB system must be captured in a tractable form. Given its pronounced nonlinearity, the system is herein represented by a simplified model, which preserves the key dynamics relevant to pressure regulation. For BLDC motor modeling, the following assumptions are made: (1) rigid mechanical coupling between the motor rotor and the pinion; (2) negligible cogging torque and gear backlash; (3) temperature effects are neglected. The dynamic behavior of the EHB system is governed by the following equation:

$$\begin{cases} J_m\ddot{\theta}_m + B_m\dot{\theta}_m = T_e - T_m - T_f \\ T_e = K_e i \\ x_m = \frac{r\theta_m}{i}, F_m = \frac{i}{r}T_m \\ m\ddot{x}_m + c\dot{x}_m + k_m x_m = F_m - P_{mc}A_{mc} \end{cases} \quad (1)$$

where J_m is the combined inertia of the motor and the pinion, B_m is the damping coefficient of the motor, θ_m is the position of the motor, T_e and T_m are the electromagnetic torque generated by the motor and the actual output torque, respectively, T_f is the friction torque, K_e is the torque coefficient, i is the current of the motor, x_m denotes the piston displacement, r represents the pinion pitch radius, i is the gear reduction ratio, and F_m is the axial thrust output from the rack-and-gear assembly. m denotes the combined mass of the rack and

piston, c is the damping coefficient of the reduction gear, and k_m represents the spring stiffness of the master cylinder. P_{mc} and A_{mc} denote the brake pressure and the effective area of the master cylinder.

By introducing a zero-velocity interval, the Karnopp model effectively eliminates the numerical 'chattering' that occurs near zero velocity, thereby ensuring numerical stability and providing a more realistic depiction of the stiction state. Furthermore, its ability to accurately capture the 'break-away' force required for the transition from stick to slip makes it particularly well-suited for characterizing friction within the EHB system:

$$T_f = \begin{cases} T_e & |\dot{\theta}_m| < \delta \& |T_e - T_m| < T_{sf} + G_f F_m \\ \left(T_{sf} + G_f F_s\right) sign(T_e - T_m) & others \\ B_t \dot{\theta}_m + \left(C_f + G_f F_s\right) sign(\dot{\theta}_m) & |\dot{\theta}_m| > \delta \end{cases} \quad (2)$$

where T_{sf} denotes the static friction torque independent of load, G_f represents the Coulomb friction torque also independent of load, and B_t is the total viscous friction coefficient of the mechanical system.

2.1. Novel P–X–V Pressure Model

The EHB's pressure–displacement relationship is strongly nonlinear and rate-dependent, making static $P_{mc} = f(x_m)$ models inadequate for dynamic braking scenarios. To capture the coupled effects of displacement and piston velocity on pressure buildup, this work adopts a $P_{mc} = f(x_m, \dot{x}_m)$ formulation, identified through experiments with varying actuation rates on the test bench (Figure 2).

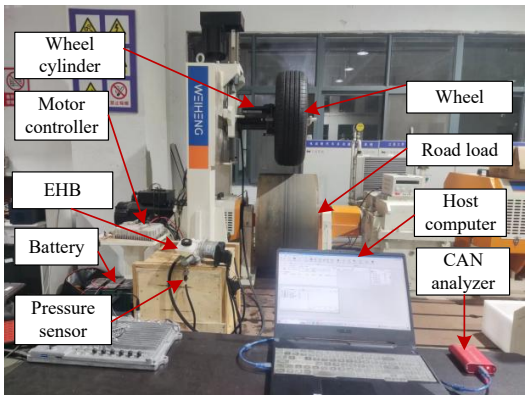

Figure 2. P–X–V characteristic test bench.

Figure 3 presents experimental results covering piston speeds from 10 mm/s to 50 mm/s, spanning the EHB's operational range. Using the 30 mm/s test as baseline, RMSE values at 50, 40, 20, and 10 mm/s are 5.33, 2.94, 2.91, and 5.54, respectively, revealing significant pressure variations outside the baseline speed. Thus, both piston displacement and velocity are essential for accurate pressure estimation and control. The master cylinder pressure model is established accordingly:

$$P_{mc} = \theta_1 (x_m - x_{dz})^2 + \theta_2 v_m \quad (3)$$

where θ_1 is the degree of concavity or convexity of the piston displacement–pressure curve, θ_2 is a positive coefficient, and x_{dz} refers to the dead zone length of the master cylinder.

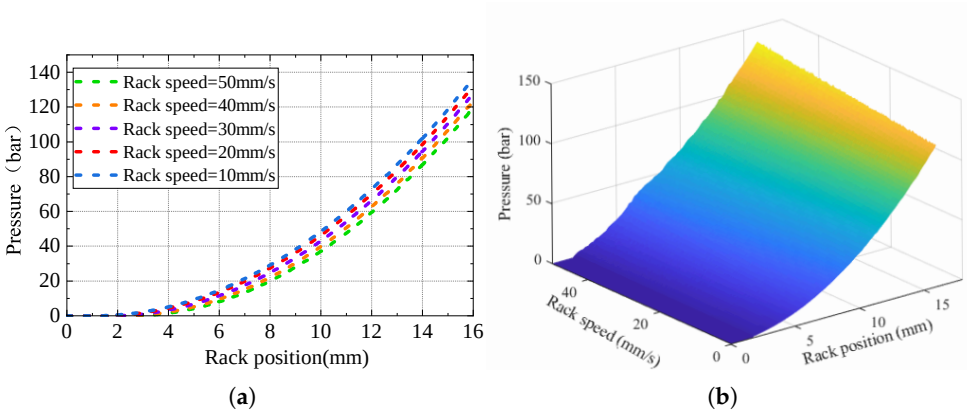

(**a**) (**b**)

Figure 3. Pressure characteristics test at each rack speed. (**a**) Pressure characteristic. (**b**) Pressure characteristic map.

2.2. Model Validation

To assess the accuracy of model, identical step and sinusoidal input commands are sent to both the test bench and the simulation models. The comparison is made between the proposed pressure model in Equation (3) and the conventional model only considering displacement x_m. As shown in Figure 4b,d, both models converge similarly at steady-state pressure. However, during dynamic pressure build-up and release phases with high piston velocity, the proposed model significantly outperforms the traditional displacement-based model, closely matching experimental data.

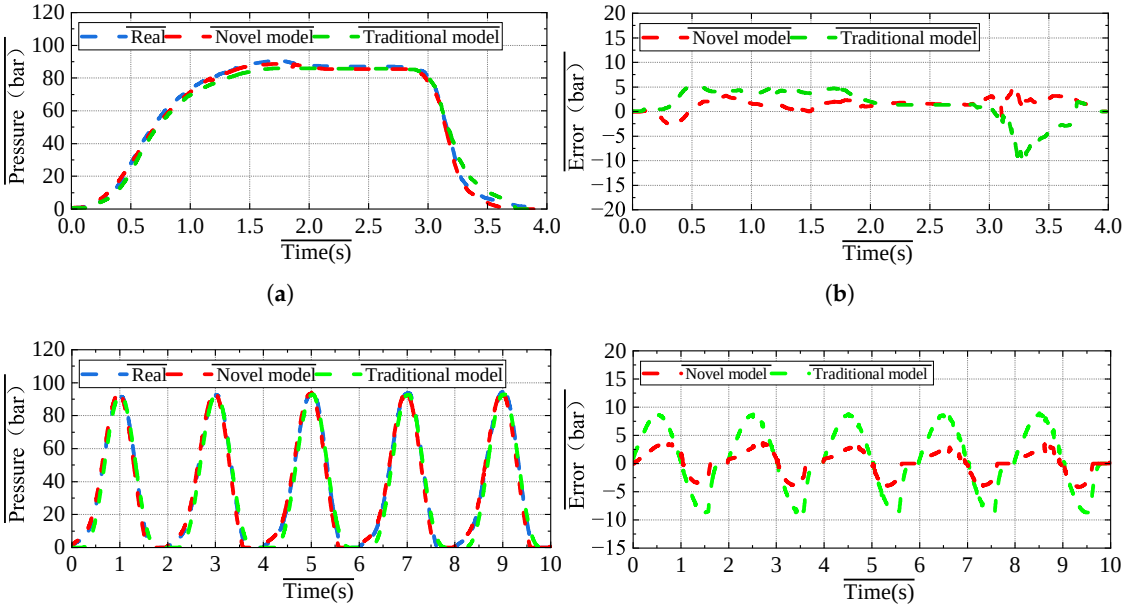

(**a**) (**b**)

(**c**) (**d**)

Figure 4. Verification of novel model. (**a**) Pressure tracking in step condition. (**b**) Pressure tracking error in step condition. (**c**) Pressure tracking in sinusoidal condition. (**d**) Pressure tracking error in sinusoidal condition.

3. Master Cylinder Pressure Estimation of EHB Based on an Extended Sliding Mode Observer

EHB systems exhibit strong nonlinear coupling across mechanical, electrical, and hydraulic domains and often operate under harsh conditions. Increasing system integration makes embedding master-cylinder pressure sensors difficult due to space and cost constraints, creating demand for sensorless pressure control strategies. Thus, an ESMO-based method is developed for high-accuracy master-cylinder pressure reconstruction, accounting

for parameter uncertainties and high-frequency disturbances. The proposed observer estimates rack position, velocity, pressure, and external disturbances simultaneously, enabling precise and robust pressure control under complex operating conditions.

State variables are chosen as $x_1 = x_m, x_2 = \dot{x}_m, y = P_{mc}$ and it can be obtained that:

$$\begin{cases} \dot{x}_1 = x_2 \\ \dot{x}_2 = \frac{1}{m}[F_m - cx_2 - k_m x_1 - A_m(\theta_1(x_1 - x_{dz})^2 + \theta_2 x_2 + \Delta_d)] \\ y = \theta_1(x_1 - x_{dz})^2 + \theta_2 x_2 + \Delta_d \end{cases} \tag{4}$$

where Δ_d denote the external disturbances term.

Assumption 1. *It is assumed that functions $f(x_1, x_2)$ are Lipschitz continuous with respect to x_1 and x_2. There exist two constants γ_1 and γ_2 satisfying the following conditions:*

$$\left| f(x_1, x_2) - \hat{f}(\hat{x}_1, \hat{x}_2) \right| = \left| \tilde{f}(\tilde{x}_1, \tilde{x}_2) \right| \leq \gamma_1 |x_1 - \hat{x}_1| + \gamma_2 |x_2 - \hat{x}_2| \tag{5}$$

Combining Equations (4) and (5), the ESMO is designed as:

$$\begin{cases} \dot{\hat{x}}_1 = \hat{x}_2 + L_1 \operatorname{sign}(x_1 - \hat{x}_1) \\ \dot{\hat{x}}_2 = \frac{1}{m}\left[F_m - c\hat{x}_2 - k_m \hat{x}_1 - A_m(\hat{\theta}_1(\hat{x}_1 - x_{dz})^2 + \hat{\theta}_2 \hat{x}_2 + \hat{\Delta}_d)\right] + L_2 \operatorname{sign}(x_2 - \hat{x}_2) \\ \hat{y} = \hat{\theta}_1(\hat{x}_1 - x_{dz})^2 + \hat{\theta}_2 \hat{x}_2 + \hat{\Delta}_d \end{cases} \tag{6}$$

where variables with hats denote estimates; L_1, L_2 are observer gains.

Define the observation error vector:

$$\tilde{X} = \begin{bmatrix} \tilde{x}_1 & \tilde{x}_2 \end{bmatrix} = \begin{bmatrix} x_1 - \hat{x}_1 & x_2 - \hat{x}_2 \end{bmatrix}$$

The error dynamics follow:

$$\begin{cases} \dot{\tilde{x}}_1 = \tilde{x}_2 - L_1 \operatorname{sign}(\tilde{x}_1) \\ \dot{\tilde{x}}_2 = -\frac{1}{m}\left[k_m \tilde{x}_1 + A_m(\tilde{\theta}_1(\tilde{x}_1 - x_{dz})^2 + \tilde{\theta}_2 \tilde{x}_2 + \tilde{\Delta}_d)\right] - L_2 \operatorname{sign}(\tilde{x}_2) \end{cases} \tag{7}$$

If the gains satisfy

$$\begin{cases} L_1 > |\tilde{x}_2| + \delta_1 \\ L_2 > \gamma_1 |\tilde{x}_1| + \gamma_2 |\tilde{x}_2| + \delta_2 \end{cases} \quad \text{with } \delta_1, \delta_2 > 0,$$

where $\gamma_1, \gamma_2 > 0$ are Lipschitz constants, then the observation error converges to zero in finite time $T > 0$:

$$\lim_{t \to T} \|\tilde{X}\| = 0.$$

Consider the Lyapunov function candidate:

$$V(\tilde{\mathbf{x}}) = \frac{1}{2}\tilde{x}_1^2 + \frac{1}{2}\tilde{x}_2^2 \tag{8}$$

The time derivative along the error trajectories satisfies:

$$\dot{V} \leq |\tilde{x}_1|(|\tilde{x}_2| - L_1) + |\tilde{x}_2|(\gamma_1 |\tilde{x}_1| + \gamma_2 |\tilde{x}_2| - L_2 + |\tilde{\Delta}_d|) < -\delta_1 |\tilde{x}_1| - \delta_2 |\tilde{x}_2| \tag{9}$$

Since $\dot{V} < -k(\delta_1, \delta_2)\|\tilde{\mathbf{x}}\|$ for some $k > 0$, the system reaches the sliding manifolds $\tilde{x}_1 = 0$ and $\tilde{x}_2 = 0$ in finite times T_1 and T_2, respectively. Convergence occurs within $T = \max\{T_1, T_2\}$.

To suppress the chattering caused by the sgn function, the discontinuous signum function is replaced by a saturation function:

$$v_{\text{mod}} = L_1 \frac{\tilde{x}_1}{|\tilde{x}_1| + \omega_1} \tag{10}$$

yielding the modified observer:

$$\begin{cases} \dot{\hat{x}}_1 = \hat{x}_2 + L_1 \dfrac{\tilde{x}_1}{|\tilde{x}_1| + \omega_1} \\ \dot{\hat{x}}_2 = \dfrac{1}{m}\left[F_m - c\hat{x}_2 - k_m\hat{x}_1 - A_m(\hat{\theta}_1(\hat{x}_1 - x_{dz})^2 + \hat{\theta}_2\hat{x}_2 + \hat{\Delta}_d)\right] + L_2 \dfrac{v_{\text{mod}}}{|v_{\text{mod}}| + \omega_2} \end{cases} \tag{11}$$

The design parameters $\omega_1, \omega_2 > 0$ provide a trade-off between convergence rate and chattering attenuation.

The adaptive laws for time-varying parameters ensure bounded estimates:

$$\begin{cases} \dot{\hat{\theta}}_1 = -k_{11}\dfrac{A_m}{m}(\hat{x}_1 - x_{dz})^2\tilde{x}_2 + \chi_1 \\ \dot{\hat{\theta}}_2 = -k_{12}\dfrac{1}{m}\tilde{x}_2^2 + \chi_2 \\ \dot{\hat{\Delta}}_d = \text{Proj}(k_{13}\tilde{x}_2) \end{cases} \tag{12}$$

where the projection operator maintains $\hat{\Delta}_d \in [\Delta_{\min}, \Delta_{\max}]$ [29]:

$$\text{Proj}(\bullet) = \begin{cases} 0 & \text{if } \hat{\Delta}_d = \Delta_{\max} \text{ and } \bullet > 0 \\ 0 & \text{if } \hat{\Delta}_d = \Delta_{\min} \text{ and } \bullet < 0 \\ \bullet & \text{otherwise} \end{cases} \tag{13}$$

4. Design of Piecewise-SMC

To enhance EHB control performance—especially rapid pressure buildup and precise tracking—this study extends the Section 3 pressure estimator by developing a Piecewise-SMC strategy that combines piecewise linear modeling with sliding mode control. This approach improves accuracy, real-time responsiveness, and robustness.

Piecewise linearization simplifies the nonlinear system into locally linear subsystems, easing modeling and controller design without losing key dynamics. Sliding mode control offers strong robustness against uncertainties and disturbances but typically suffers from chattering, which degrades performance and stability.

The proposed Piecewise-SMC balances model fidelity and implementation simplicity. It uses desired master cylinder pressure as the reference and feedback from motor angle, velocity, and estimated pressure. Unlike polynomial models that lack physical interpretability and complicate controller design, piecewise linear fitting captures the full $\dot{P}_{mc}$–x_m–v_m behavior across the operating range, segmented by piston displacement x_m. The fitting results appear in Figure 5.

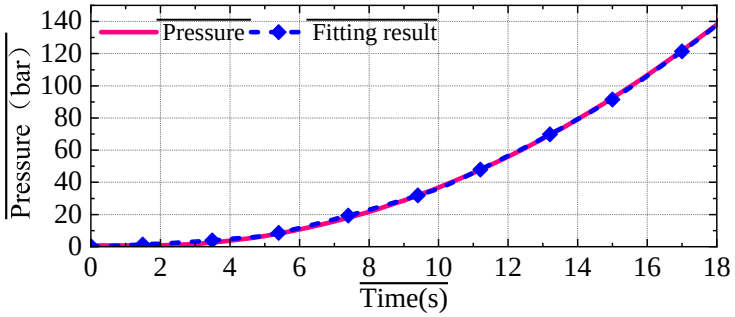

Figure 5. The pressure fitting result.

Therefore, the pressure–position–velocity model can be expressed as:

$$\dot{p}_{mc\_k} = a_k x_{m\_k} + b_k v_{m\_k}, \quad 1 \leq k \ \leq n \tag{14}$$

where a_k, b_k is the fitting coefficient.

Then, the state space expression can be obtained as follows:

$$\dot{x} = Ax + Bu \tag{15}$$

where

$$\begin{gathered} x = \begin{bmatrix} x_1 & x_2 & x_3 \end{bmatrix}^T = \begin{bmatrix} x_m & \dot{x}_m & p_{mc} \end{bmatrix}^T \quad u = [T_e - T_f] \\ A = \begin{bmatrix} 0 & 2 & 0 \\ -\frac{\xi_3}{\xi_1} & -\frac{\xi_2}{\xi_1} & -\frac{\xi_4}{\xi_1} \\ a_k & b_k & 0 \end{bmatrix} \qquad B = \begin{bmatrix} -1 \\ 0 \\ 0 \end{bmatrix} \end{gathered} \tag{16}$$

$$\begin{bmatrix} \xi_1 & \xi_2 \\ \xi_3 & \xi_4 \end{bmatrix} = \begin{bmatrix} \frac{i}{r}\eta J_m + \frac{mr}{i\eta} & \frac{i}{r}\eta B_m + \frac{cr}{i\eta} \\ \frac{kr}{i\eta} & \frac{A_m r}{i\eta} \end{bmatrix} \tag{17}$$

The reference pressure is defined as x_{3d}, and the pressure error can be defined as e_3:

$$e_3 = x_3 - x_{3d} \tag{18}$$

The sliding mode surface can be defined as:

$$s = (\dot{x}_3 - \dot{x}_{3d}) + \lambda(x_3 - x_{3d}), \lambda > 0 \tag{19}$$

where, the choice of λ depends on system characteristics and is often fine-tuned through simulations and experiments to achieve satisfactory robustness and responsiveness.

Then, the derivative of s can be concluded that:

$$\begin{gathered} \dot{s} = (a_k + b_k\lambda - b_k\tfrac{\xi_2}{\xi_1})x_2 - b_k\tfrac{\xi_4}{\xi_1}\left[\theta_1(x_1 - x_{dz})^2 + \theta_2 x_2 + \Delta\right] \\ +(a_k\lambda - b_k\tfrac{\xi_3}{\xi_1})x_1 + b_k u - \ddot{x}_{3d} - \lambda\dot{x}_{3d} \end{gathered} \tag{20}$$

Let

$$\dot{s} = -\varepsilon sign s - ks \tag{21}$$

The control law u is designed as:

$$u = \frac{1}{b_k}\begin{bmatrix} -(a_k\lambda - b_k\frac{\xi_3}{\xi_1})x_1 - (a_k + b_k\lambda - b_k\frac{\xi_2}{\xi_1})x_2 \\ +b_k\frac{\xi_4}{\xi_1}\left[\hat{\theta}_1(x_1 - x_{dz})^2 + \hat{\theta}_2 x_2 + \hat{\Delta}\right] + \ddot{x}_{3d} \\ +\lambda\dot{x}_{3d} - \varepsilon sign s - ks \end{bmatrix} \tag{22}$$

where ε and k are both positive constants, with ε satisfying the following conditions:

$$\varepsilon > b_k \frac{\xi_4}{\xi_1} |\tilde{\Delta}|_{\max} \tag{23}$$

By substituting Equation (22) into Equation (20), it can be obtained that:

$$\dot{s} = -b_k \frac{\xi_4}{\xi_1} \left[\hat{\theta}_1 (x_1 - x_{dz})^2 + \hat{\theta}_2 x_2 + \hat{\Delta} \right] - \varepsilon sign s - ks \tag{24}$$

Define the Lyapunov function as:

$$V_2 = \frac{1}{2}\tilde{x}_1^2 + \frac{1}{2}\tilde{x}_2^2 + \frac{1}{2}k_{11}^{-1}\tilde{\theta}_1^2 + \frac{1}{2}k_{12}^{-1}\tilde{\theta}_2^2 + \frac{1}{2}k_{13}^{-1}\tilde{\Delta}^2 + \frac{1}{2}k_h^{-1}s^2 \tag{25}$$

where $\frac{1}{2}\tilde{x}_1^2 + \frac{1}{2}\tilde{x}_2^2$ measures the energy of the state observation error; $\frac{1}{2}{k_{11}}^{-1}\tilde{\theta}_1^2 + \frac{1}{2}{k_{12}}^{-1}\tilde{\theta}_2^2 + \frac{1}{2}{k_{13}}^{-1}\tilde{\Delta}^2$ measures the energy of the parameter/disturbance identification error; $\frac{1}{2}k_h^{-1}s^2$ measures the energy of the sliding mode control tracking error; k_h is a positive constant.

Based on the result of Equation (11), the time derivative of V_2 along the system is obtained as:

$$\begin{array}{l} \dot{V}_2 = \tilde{x}_1\dot{\tilde{x}}_1 + \tilde{x}_2\dot{\tilde{x}}_2 - k_{11}^{-1}\tilde{\theta}_1\chi_1 - k_{12}^{-1}\tilde{\theta}_2\chi_2 + \tilde{\Delta}\left[\tilde{x}_2 - k_{13}^{-1}\dot{\hat{\Delta}}\right] \\ +k_h^{-1}\left[-b_k\frac{\xi_4}{\xi_1}\left[\hat{\theta}_1(x_1 - x_{dz})^2 + \hat{\theta}_2 x_2 + \hat{\Delta}\right]s - \varepsilon|s| - ks^2 \right] \end{array} \tag{26}$$

Then, select additional correction terms χ_1, χ_2 as

$$\begin{cases} \chi_1 = -k_{11}k_h^{-1}b_k\frac{\xi_4}{\xi_1}(\tilde{x}_1 - x_{dz})^2 s \\ \chi_2 = -k_{12}k_h^{-1}b_k\frac{\xi_4}{\xi_1}\tilde{x}_2 s \end{cases} \tag{27}$$

Substituting Equation (27) into Equation (26) yields:

$$\dot{V}_2 = \tilde{x}_1\dot{\tilde{x}}_1 + \tilde{x}_2\dot{\tilde{x}}_2 + \tilde{\Delta}\left[\tilde{x}_2 - k_{13}^{-1}\dot{\hat{\Delta}}\right] + k_h^{-1}\left[-b_k\frac{\xi_4}{\xi_1}\hat{\Delta}s - \varepsilon|s| - ks^2\right] \tag{28}$$

Then, it can be obtained that $\tilde{x}_1\dot{\tilde{x}}_1 < \delta_1|\tilde{x}_1| \le 0$, $\tilde{x}_2\dot{\tilde{x}}_2 < \delta_2|\tilde{x}_2| \le 0$, $\tilde{\Delta}\left[\tilde{x}_2 - k_{13}^{-1}\dot{\hat{\Delta}}\right] \le 0$, $-b_k\frac{\xi_4}{\xi_1}\hat{\Delta}s - \varepsilon|s| \le 0$. Then, the following conclusion can be derived as:

$$\dot{V}_2 = -k_h^{-1}ks^2 \le 0 \tag{29}$$

This ensures the stability of the overall closed-loop system composed of the Piecewise-SMC controller and the ESMO under closed-loop operation, as well as the boundedness of system signals.

Since the system is partitioned into subsystems and the sliding mode sign function induces high-frequency chattering, it is replaced with a saturation function to enhance control performance. Equation (24) is thus rewritten as:

$$u = \frac{1}{b_k}\begin{bmatrix} -(a_k\lambda - b_k\frac{\xi_3}{\xi_1})x_1 - (a_k + b_k\lambda - b_k\frac{\xi_2}{\xi_1})x_2 \\ +b_k\frac{\xi_4}{\xi_1}\left[\hat{\theta}_1(x_1 - x_{dz})^2 + \hat{\theta}_2 x_2 + \hat{\Delta}\right] + \ddot{x}_{3d} \\ +\lambda\dot{x}_{3d} - \varepsilon sat\left(\frac{\sigma}{\phi}\right) - ks \end{bmatrix} \tag{30}$$

where ϕ is the thickness of the boundary layer, $\phi \ge 0$.

$$sat(\sigma/\phi) = \begin{cases} \sigma/\phi, |\sigma/\phi| < 1 \\ \mathrm{sgn}(\sigma/\phi), |\sigma/\phi| \ge 1 \end{cases} \tag{31}$$

The proposed Piecewise-SMC framework (Figure 6) builds on a high-fidelity P–V–P model to capture nonlinear dynamics, employs an ESMO for real-time state estimation under uncertainties and sensorless conditions, and uses a piecewise affine approximation to enable tractable controller design. These components jointly support subsystem-specific sliding mode laws, achieving robust and precise pressure regulation across the EHB operating range.

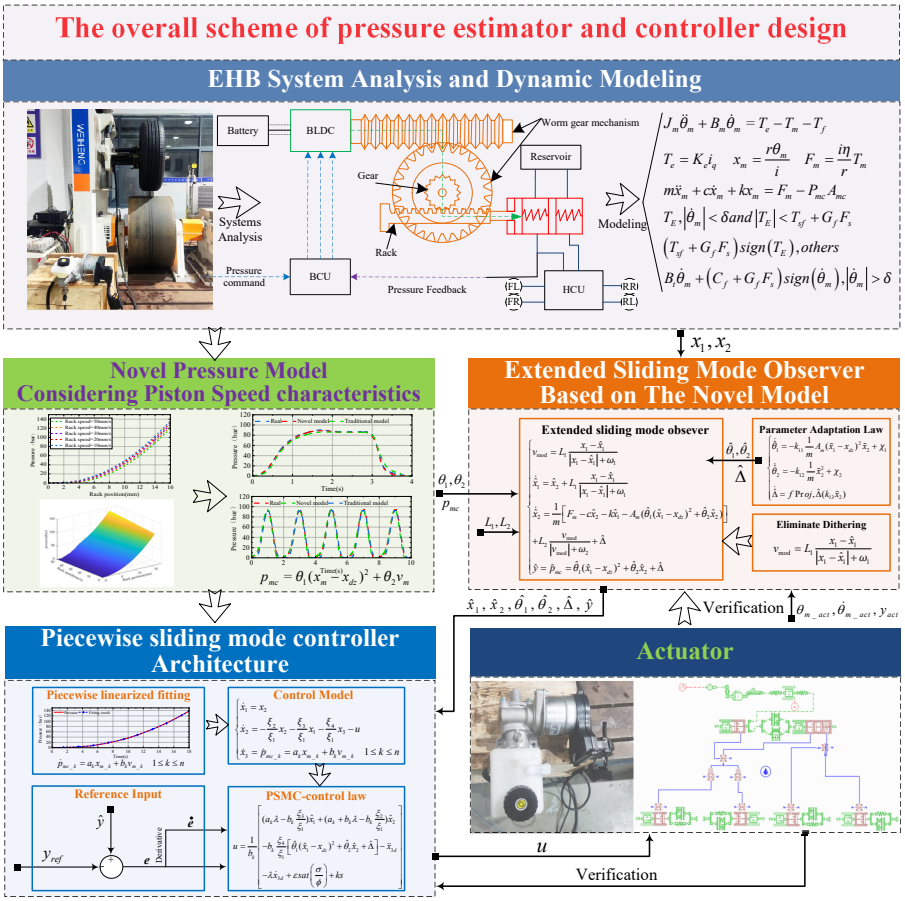

Figure 6. The overall scheme of pressure estimator and controller design.

5. Results and Analysis

To verify the performance of the proposed ESMO pressure estimator and Piecewise-SMC pressure controller, simulations and experiments are conducted.

5.1. Simulation Results of Master Cylinder Pressure Estimation

Under typical braking conditions, the performance of ESMO is evaluated through simulation. To assess the practical applicability of the proposed pressure estimator, it is integrated into a closed-loop control system, wherein a Piecewise-SMC strategy is employed to achieve accurate tracking of the master cylinder pressure.

Figure 7 presents the pressure estimation results of the ESMO and the corresponding tracking performance of the controller under various operating scenarios. The root mean square errors (RMSE) of the ESMO under two distinct conditions are 0.1764 bar and 0.2368 bar, respectively. The mean estimation error is −0.0160 bar, and the maximum absolute error reaches 1.2249 bar. These results demonstrate that the ESMO exhibits strong dynamic estimation capability and high steady-state accuracy, thereby meeting the performance requirements of the closed-loop controller.

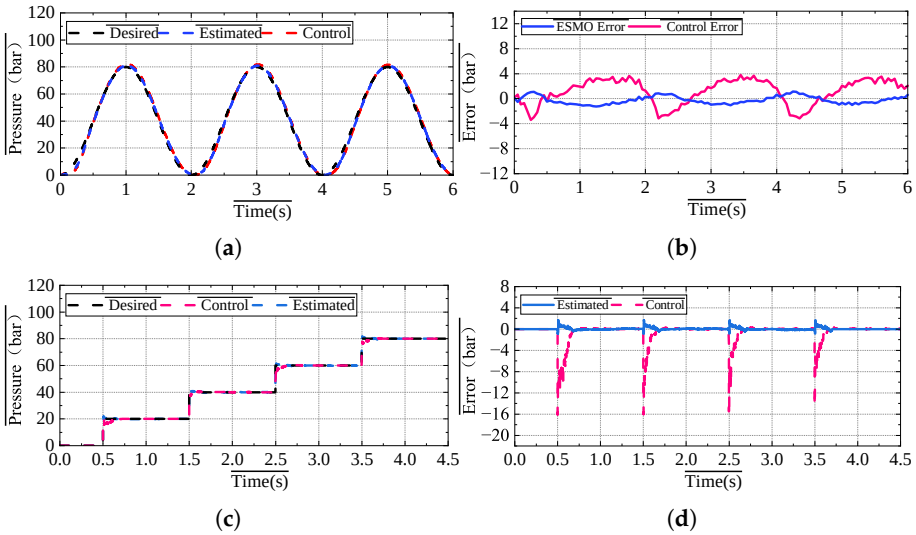

Figure 7. Simulation of master cylinder pressure estimation. (**a**) Estimated in sinusoidal condition. (**b**) Estimated error in sinusoidal condition. (**c**) Estimated in step condition. (**d**) Estimated error in step condition.

5.2. Simulation Results of Pressure Control Strategy

This section also designs two benchmark controllers for comparison: an SMC controller based on the conventional EHB model and a Piecewise-PID controller based on the proposed pressure model. These benchmark controllers are used to validate the effectiveness and advantages of the proposed Piecewise-SMC control strategy. The corresponding simulation results and performance analyses are presented in Figure 8.

Figure 8 illustrates the simulation results of the Piecewise-SMC, SMC, and Piecewise-PID controllers under sinusoidal and step braking conditions. As shown in Figure 8b, under the sinusoidal condition, the Piecewise-SMC controller achieves an RMSE of 2.31 bar and a maximum absolute error of 3.77 bar. Under the step condition (Figure 8e), the Piecewise-SMC achieves an RMSE of 2.17 bar, with a maximum overshoot of 2.17% and an average response time of 0.12 s. These results clearly demonstrate that, compared with the SMC and Piecewise-PID controllers, the proposed Piecewise-SMC controller offers superior performance in mitigating the effects of system uncertainties and external disturbances during the pressure regulation process. Furthermore, it achieves faster dynamic response while enhancing the system's robustness and tracking accuracy.

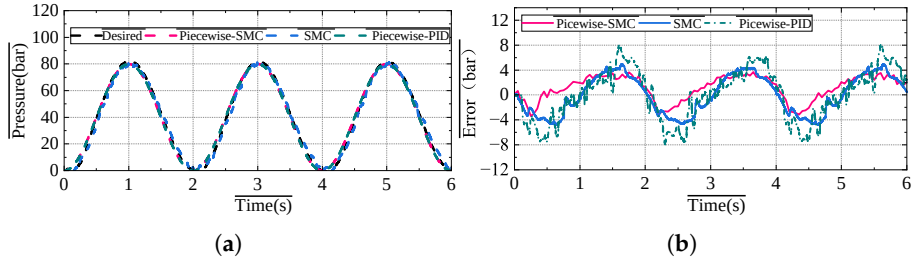

Figure 8. *Cont.*

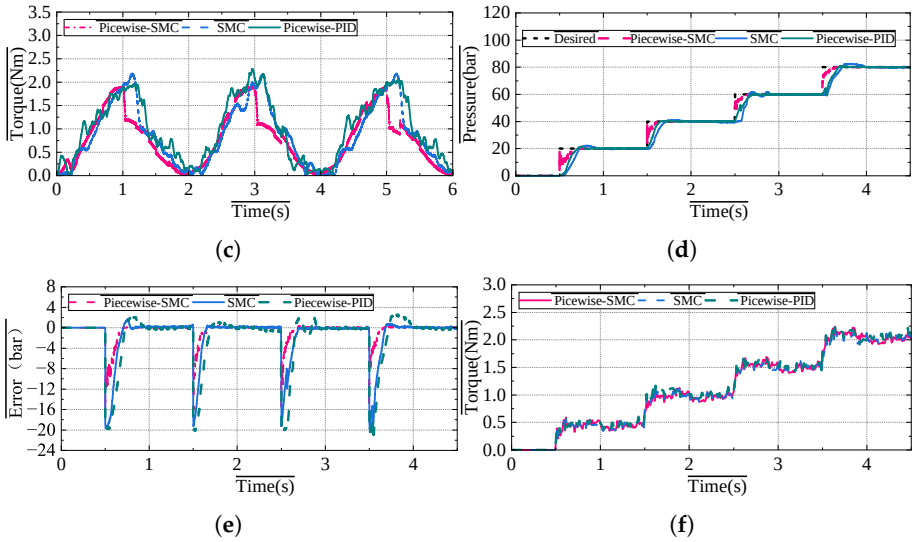

Figure 8. Simulation of MCPE. (**a**) Pressure tracking in sinusoidal condition. (**b**) Tracking error in sinusoidal condition. (**c**) Motor torque in sinusoidal condition. (**d**) Pressure tracking in step condition. (**e**) Tracking error in step condition. (**f**) Motor torque in step condition.

5.3. Results of Experimental Verification

To further validate the effectiveness of the proposed control system in practical applications, the Piecewise-SMC strategy is experimentally tested on an EHB test bench, as shown in Figure 9.

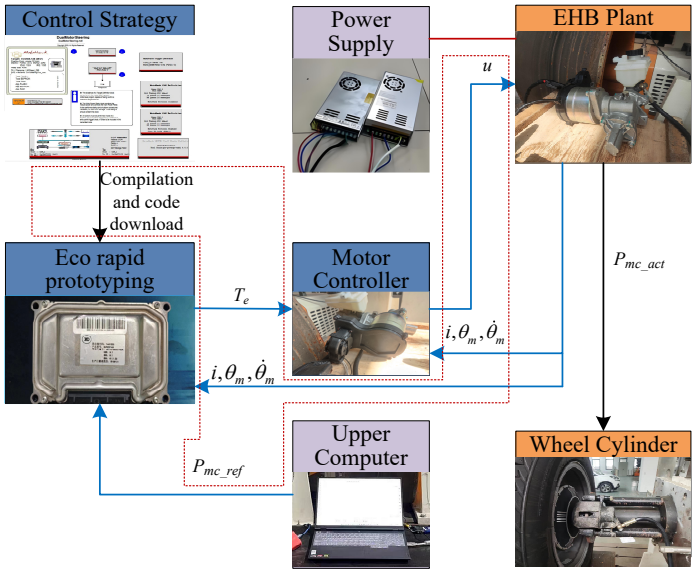

Figure 9. EHB test bench of experimental validation.

Two braking scenarios—sinusoidal and step-change—simulate real vehicle conditions, with pressure tracking results in Figure 10. Under the sinusoidal profile (Figure 10a,c), all controllers show tracking errors, but Piecewise-SMC outperforms others. Its steady-state RMSEs are 4.63 bar, 7.69 bar, and 9.06 bar for Piecewise-SMC, SMC, and Piecewise-PID, respectively, reflecting reductions of 39.8% and 48.9%. Maximum absolute errors are reduced by 33.2% and 50.6% accordingly.

In the step response (Figure 10b,d), Piecewise-SMC achieves 0.15 s response time, 4.37% overshoot, and 6.45 bar RMSE, improving over SMC (0.22 s, 6.81%, 7.13 bar) and Piecewise-PID (0.31 s, 10.01%, 7.95 bar). Compared to SMC, Piecewise-SMC reduces

response time, overshoot, and RMSE by 31.8%, 35.8%, and 9.6%; against Piecewise-PID, reductions reach 51.6%, 56.3%, and 18.9%. Experimental results differ from simulations due to external disturbances and communication delays. Nonetheless, bench tests confirm Piecewise-SMC's superior robustness and dynamic response over SMC and Piecewise-PID.

Quantitative results are shown in Table 2. In summary, Piecewise-SMC's advantage over traditional SMC arises from the accurate piecewise model enhancing control precision, while compared to Piecewise-PID, its sliding mode control ensures stronger robustness and better dynamic performance under uncertainties.

Table 2. Quantitative results of experiments.

Conditions	Indices	Piecewise-SMC	SMC	Piecewise-PID
Sinusoidal	RMSE (bar)	4.63	7.69	9.06
	MAE (bar)	9.51	14.23	19.23
Step	RMSE (bar)	6.45	7.13	7.95
	Average Overshoot (%)	4.37%	6.81%	10.01%
	Average Response Time (s)	0.15	0.22	0.31

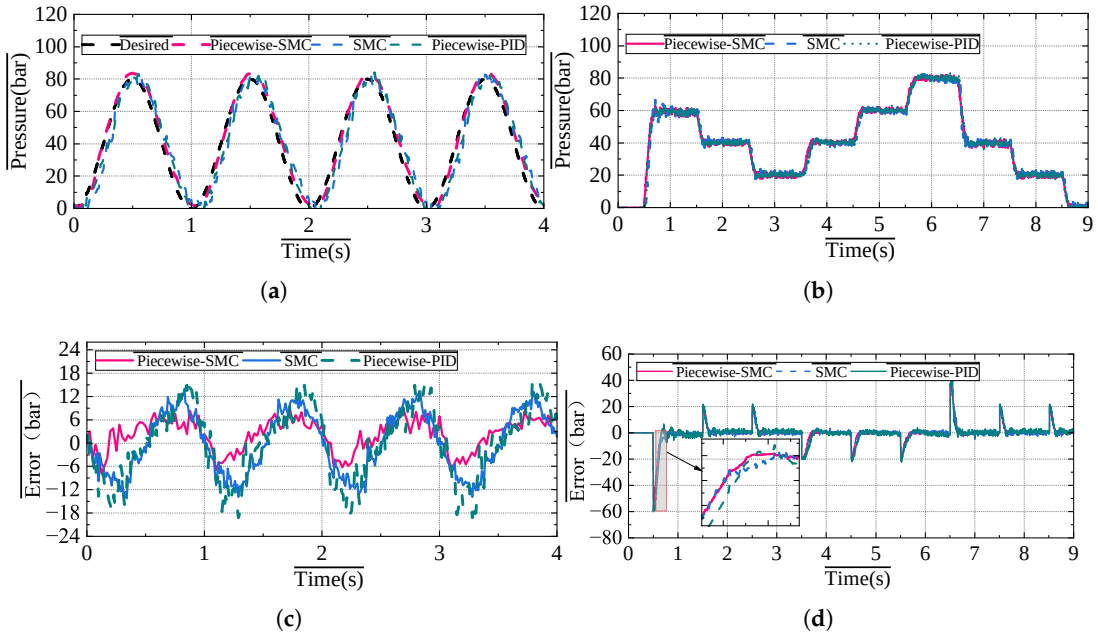

Figure 10. Experiment of pressure-tracking. (**a**) Pressure tracking in sinusoidal condition. (**b**) Tracking error in stair-step condition. (**c**) Pressure tracking error in sinusoidal condition. (**d**) Pressure tracking error in stair-step condition.

6. Conclusions

This paper develops a master cylinder pressure estimation and tracking control method for EHB systems, with key conclusions as follows:

(1) A dynamic model incorporating piston velocity is established, enhancing pressure representation beyond traditional displacement-only models and improving dynamic response.

(2) An ESMO is designed based on this model to estimate pressure without sensors, effectively handling nonlinearities and uncertainties with high accuracy and robustness under realistic braking.

(3) Building on the model and observer, a Piecewise-SMC controller is proposed. Experiments under step braking scenarios show the Piecewise-SMC reduces RMSE by up

to 9.6%, response time by 31.8%, and overshoot by 35.8% compared to conventional SMC, demonstrating notable gains in tracking accuracy and dynamic performance.

Future work includes extending the controller to fixed-time convergence [30], integrating machine learning for adaptability, and leveraging quantum computing for advanced control optimization.

Author Contributions: Conceptualization, C.L. and H.D.; methodology, C.L.; validation, C.L., Y.W. and H.D.; writing—original draft preparation, C.L., H.D. and C.H.; writing—review and editing, X.X.; supervision, L.C.; project administration, X.X.; funding acquisition, X.X. All authors have read and agreed to the published version of the manuscript.

Funding: This work was supported by the National Natural Science Foundation of China (Grant No. 52225212) and the Jiangsu Provincial Key Research and Development Program (Grant No. BE2019010).

Data Availability Statement: Data are contained within the article.

Conflicts of Interest: The authors declare that the research was conducted in the absence of any commercial or financial relationships that could be construed as a potential conflict of interest.

References

1. Zhang, Q.; Jin, L.; Zhang, Y.; Li, J. Research on Estimation and Precise Control of Wheel Cylinder Pressure for Integrated Electronic Hydraulic Brake System. In Proceedings of the 2021 China Automation Congress (CAC), Beijing, China, 22–24 October 2021; IEEE: New York, NY, USA, 2021; pp. 4590–4594.
2. Wei, L.; Liu, Y.; Zhu, Z.; Wang, X.; Li, L. Parameters self-learning of solenoid valve for wheel pressure estimation. *Proc. Inst. Mech. Eng. Part D J. Automob. Eng.* **2024**, *238*, 3109–3120. [CrossRef]
3. Tang, Z.; Zhang, H.; Li, H.; Li, Y.; Ding, Z.; Chen, J. Development of crawler steering gearbox for combine harvester straight forward and steering in situ. *Int. J. Agric. Biol. Eng.* **2020**, *13*, 120–126. [CrossRef]
4. Chen, J.; Zong, H.; Song, H.; Wu, Y.; Liang, H.; Su, Z. Closed-loop plasma flow control of a turbulent cylinder wake flow using machine learning at Reynolds number of 28,000. *Phys. Fluids* **2024**, *36*, 015123. [CrossRef]
5. Wei, L.; Liu, Y.; Wang, X.; Li, L. Estimation of Wheel Pressure for Hydraulic Braking System by Interacting Multiple Model Filter. *IEEE Trans. Veh. Technol.* **2024**, *73*, 463–472. [CrossRef]
6. Chen, Y.; Chen, L.; Wang, R.; Xu, X.; Shen, Y.; Liu, Y. Modeling and test on height adjustment system of electrically-controlled air suspension for agricultural vehicles. *Int. J. Agric. Biol. Eng.* **2016**, *9*, 40–47.
7. Chen, Y.; Chen, L.; Huang, C.; Lu, Y.; Wang, C. A dynamic tire model based on HPSO-SVM. *Int. J. Agric. Biol. Eng.* **2019**, *12*, 36–41. [CrossRef]
8. Li, H.; Yu, Z.; Xiong, L.; Han, W. *Hydraulic Control of Integrated Electronic Hydraulic Brake System Based on Lugre Friction Model*; Technical Report; SAE Technical Paper; SAE: Warrendale, PA, USA, 2017.
9. Liu, H.; Yan, S.; Shen, Y.; Li, C.; Zhang, Y.; Hussain, F. Model predictive control system based on direct yaw moment control for 4WID self-steering agriculture vehicle. *Int. J. Agric. Biol. Eng.* **2021**, *14*, 175–181. [CrossRef]
10. Zheng, J.; Nie, S.; Jing, H.; He, Y.; Li, M.; Ma, Y.; Ding, Z. Potential and electro-mechanical coupling analysis of a novel HTS maglev system employing double-sided homopolar linear synchronous motor. *IEEE Trans. Intell. Transp. Syst.* **2024**, *25*, 13573–13583. [CrossRef]
11. Jiang, L.; Shi, Q.; Wei, Y.; He, Y.; He, Z.; He, L. Electro-hydraulic braking dynamics for pressure demand control of brake-by-wire system. *Proc. Inst. Mech. Eng. Part D J. Automob. Eng.* **2024**, *238*, 735–748. [CrossRef]
12. Xiong, L.; Han, W.; Yu, Z. Adaptive sliding mode pressure control for an electro-hydraulic brake system via desired-state and integral-antiwindup compensation. *Mechatronics* **2020**, *68*, 102359. [CrossRef]
13. Shi, B.; Xiong, L.; Yu, Z. Master Cylinder Pressure Estimation of the Electro-Hydraulic Brake System Based on Modeling and Fusion of the Friction Character and the Pressure-Position Character. *IEEE Trans. Veh. Technol.* **2022**, *72*, 1748–1762. [CrossRef]
14. Shi, Q.; He, L. A model predictive control approach for electro-hydraulic braking by wire. *IEEE Trans. Ind. Inform.* **2022**, *19*, 1380–1388. [CrossRef]
15. Todeschini, F.; Corno, M.; Panzani, G.; Fiorenti, S.; Savaresi, S.M. Adaptive cascade control of a brake-by-wire actuator for sport motorcycles. *IEEE/ASME Trans. Mechatron.* **2014**, *20*, 1310–1319. [CrossRef]
16. Wang, X.; Wu, X.; Cheng, S.; Shi, J.; Ping, X.; Yue, W. Design and experiment of control architecture and adaptive dual-loop controller for brake-by-wire system with an electric booster. *IEEE Trans. Transp. Electrif.* **2020**, *6*, 1236–1252. [CrossRef]

17. Cheng, Z.; Li, L.; Liu, X.; Bai, X.; Liu, J. Sensorless Control Based on Discrete Fractional-Order Terminal Sliding Mode Observer for High-Speed PMSM with LCL Filter. *IEEE Trans. Power Electron.* **2025**, *40*, 1654–1668. [CrossRef]
18. Liu, F.; Zhao, X.; Zhu, Z.; Zhai, Z.; Liu, Y. Dual-microphone active noise cancellation paved with Doppler assimilation for TADS. *Mech. Syst. Signal Process.* **2023**, *184*, 109727. [CrossRef]
19. Shi, B.; Xiong, L.; Yu, Z. Pressure estimation of the electro-hydraulic brake system based on signal fusion. *Actuators* **2021**, *10*, 240. [CrossRef]
20. Wei, H.; Xiong, L.; Yu, Z. *Braking Pressure Tracking Control of a Pressure Sensor Unequipped Electro-Hydraulic Booster Based on a Nonlinear Observer*; Technical Report; SAE Technical Paper; SAE: Warrendale, PA, USA, 2018.
21. Chen, G.; Wu, W.; Yang, C.; Hu, H.; Zhang, J.; Shi, J.; Wu, C.; Ma, Y. Practical Finite-Time Observer-Based Adaptive Backstepping Super-Twisting Sliding Mode Control for Deep-Sea Hydraulic Manipulator. *IEEE Trans. Ind. Electron.* **2025**, *72*, 9569–9579. [CrossRef]
22. Razmjooei, H.; Palli, G.; Strano, S.; Tordela, C. Development of sliding mode observers for estimating sideslip angle and lateral forces in road vehicles. *Trans. Inst. Meas. Control* **2025**, 01423312251326643. [CrossRef]
23. Wang, K.; Liu, X.; Wang, G. Self-scheduled direct thrust control for gas turbine engine based on EME approach with bounded parameter variation. *Chin. J. Aeronaut.* **2025**, *38*, 103392. [CrossRef]
24. Ding, S.; Liu, C.; Fan, Z.; Hang, J. Lumped Parameter Adaptation-Based Automatic MTPA Control for IPMSM Drives by Using Stator Current Impulse Response. *IEEE Trans. Energy Convers.* **2025**, *40*, 2108–2118. [CrossRef]
25. Zhang, S.; He, Y.; Gu, Y.; He, Y.; Wang, H.; Wang, H.; Yang, R.; Chady, T.; Zhou, B. UAV based defect detection and fault diagnosis for static and rotating wind turbine blade: A review. *Nondestruct. Test. Eval.* **2025**, *40*, 1691–1729. [CrossRef]
26. Han, W.; Xiong, L.; Yu, Z. Interconnected pressure estimation and double closed-loop cascade control for an integrated electrohydraulic brake system. *IEEE/ASME Trans. Mechatron.* **2020**, *25*, 2460–2471. [CrossRef]
27. Han, W.; Xiong, L.; Yu, Z.; Zhuo, G.; Leng, B.; Xu, S. Integrated pressure estimation and control for electro-hydraulic brake systems of electric vehicles considering actuator characteristics and vehicle longitudinal dynamics. *IEEE/ASME Trans. Mechatron.* **2022**, *28*, 197–209. [CrossRef]
28. Gao, Z.; Yang, Y.; Chen, G.; Yuan, L.; Zhou, J.; Zhang, J. Adaptative Pressure Estimation and Control Architecture for Integrated Electro-Hydraulic Brake System. *Chin. J. Mech. Eng.* **2025**, *38*, 28. [CrossRef]
29. Chen, Z.; Huang, C.; Liu, Z.; Liu, Y.; Wang, X.; Shi, B.; Li, L. An Offset-Free Explicit Model Predictive Pressure Controller for Integrated Braking System. *IEEE Trans. Transp. Electrif.* **2024**, *10*, 2355–2366. [CrossRef]
30. Ning, B.; Han, Q.L.; Ding, L. A Brief Overview of Recent Advances in Distributed Accelerated Secondary Control for Islanded AC Microgrids. *IEEE Trans. Ind. Inform.* **2025**. [CrossRef]